Pressure Study of the Thermal Spin Transition and the High-Spin → Low-Spin Relaxation in the $R\bar{3}$ and $P\bar{1}$ Crystallographic Phases of $[Zn_{1-x}Fe_x(ptz)_6](BF_4)_2$ Single Crystals ($x = 0.1$, 0.32, and 1; ptz = 1-*n*-propyltetrazole)

Jelena Jeftić[†] and Andreas Hauser*[,‡]

Departement für Chemie und Biochemie, Universität Bern, Freiestrasse 3, CH-3000 Bern 9, Switzerland, and Département de Chimie Physique, Université de Genève, 30 Quai Ernest-Ansermet, CH-1211 Genève 4, Switzerland

Received: June 25, 1997; In Final Form: September 30, 1997[⊗]

In the iron(II) spin-crossover compound $[Fe(ptz)_6](BF_4)_2$, the thermal spin transition is accompanied by a crystallographic phase transition showing a hysteresis with $T_c^{\downarrow} = 128$ K and $T_c^{\uparrow} = 135$ K at ambient pressure [Franke, P. L.; Haasnot, J. G.; Zuur, A. P. *Inorg. Chim. Acta* **1982**, *59*, 5]. The hysteresis is due to an interplay between the spin-transition and the $R\bar{3} \rightarrow P\bar{1}$ crystallographic phase transition with a large low-spin fraction stabilizing the $P\bar{1}$ phase at low temperatures. In the mixed crystal $[Zn_{1-x}Fe_x(ptz)_6](BF_4)_2$, $x = 0.1$, with the iron complexes imbedded into the isomorphous zinc lattice, the crystallographic phase transition can be induced by an external pressure [Jeftić, J.; Romstedt, H.; Hauser, A. *J. Phys. Chem. Solids* **1996**, *57*, 1743]. Thus the $P\bar{1}$ phase is additionally stabilized by external pressure. The interaction constant Γ, which describes cooperative effects between the spin-changing complexes, differs for the two crystallographic phases. Values for $\Gamma(P\bar{1})$ of 144(8) cm^{-1} and the volume difference ΔV°_{HL} of 29(4) $Å^3$ are determined from a simultaneous fit to a series of transition curves for different pressures and iron content x in the $P\bar{1}$ phase. These values are compared to the corresponding values for the $R\bar{3}$ phase, viz. $\Gamma(R\bar{3})$ of 170(9) cm^{-1} and $\Delta V^{\circ}_{HL}(R\bar{3})$ of 26(3) $Å^3$. Surprisingly $\Gamma(R\bar{3})$ is larger than $\Gamma(P\bar{1})$ despite the fact that $\Delta V^{\circ}_{HL}(R\bar{3})$ is smaller than $\Delta V^{\circ}_{HL}(P\bar{1})$. The high-spin → low-spin relaxation at temperatures above ~80 K is thermally activated, while below ~40 K temperature independent tunnelling takes place. An external pressure of 1 kbar accelerates the high-spin → low-spin relaxation exponentially by 1 order of magnitude in the tunnelling region in both crystallographic phases and regardless of x. In the concentrated material the high-spin → low-spin relaxation is self-accelerating due a buildup of an internal pressure [Hauser, A. *Chem. Phys. Lett.* **1992**, *192*, 65]. Both cooperative effects and external pressure result in a shift of the maximum of the $^1A_1 \rightarrow {}^1T_1$ absorption band.

1. Introduction

Iron(II) complexes which show a thermal spin transition from the $^1A_1$ low-spin (LS) state at low temperatures to the $^5T_2$ high-spin (HS) state at elevated temperatures, so called spin-crossover complexes,[1] are the subject of much current work. They are particularly well suited for pressure studies[3,4] because the difference in volume, $\Delta V^{\circ}_{HL} = V_{HS} - V_{LS}$, between HS and LS complexes is comparatively large due to the large difference in metal−ligand bond lengths, $\Delta r^{\circ}_{HL} = r_{HS} - r_{LS} \approx 0.16-0.21$ Å.[5] Therefore, the contribution of the work term, $p\Delta V^{\circ}_{HL}$, to the Gibbs' free energy is already significant for comparatively small external pressures of up to 1000 bar.[6−8] In addition to influencing the spin equilibrium, external pressures also affect the kinetics of the HS → LS relaxation.[9−11]

In the iron(II) spin-crossover compound $[Fe(ptz)_6](BF_4)_2$ (ptz = 1-*n*-propyltetrazole) the thermal spin transition is accompanied by a crystallographic phase transition with $T_c^{\downarrow} = 128$ K and $T_c^{\uparrow} = 135$ K at ambient pressure.[12] The crystal is in space group $R\bar{3}$ at temperatures above $T_c^{\uparrow}$ and in $P\bar{1}$ below $T_c^{\downarrow}$.[13] The thermal spin transition in both phases is quite abrupt due to the cooperative effects of elastic origin present in such a neat spin-crossover crystal. Upon fast cooling, the crystallographic phase transition is suppressed, and the crystal remains in the $R\bar{3}$ space group even below $T_c^{\downarrow}$.[14,15] In the diluted mixed crystal $[Zn_{1-x}Fe_x(ptz)_6](BF_4)_2$, $x = 0.1$, the spin transition is gradual, as expected in the absence of cooperative effects. But even then it is possible to induce the crystallographic phase transition by external pressure.[8]

A general discussion of intersystem crossing in iron(II) spin-crossover compounds as a model process between classical and quantum mechanical behavior has been given in ref 16. The HS → LS relaxation at cryogenic temperatures of the concentrated title compound in the $R\bar{3}$ phase at ambient pressure following the quantitative light-induced population of the HS state as metastable state has previously been studied. The sigmoidal, self-accelerated relaxation curves[17] were attributed to a buildup of an internal pressure due the elastic interaction during the relaxation process. In the diluted system $[Zn_{1-x}Fe_x(ptz)_6](BF_4)_2$, $x = 0.1$, a study of the HS → LS relaxation under external pressure was performed. An external pressure of 1000 bar accelerates the relaxation in the dilute system by 1 order of magnitude.[11]

The present study focuses on the interplay between the thermal spin transition and the crystallographic phase transition in the mixed crystal system $[Zn_{1-x}Fe_x(ptz)_6](BF_4)_2$, $x = 0.1$, 0.32, and 1. An accurate determination of the thermodynamic parameters in both crystallographic phases is presented, and the elastic interactions are discussed within a mean-field approach. Furthermore, the HS → LS relaxation has been studied at temperatures between 15 and 70 K as well as at elevated pressures of up to 1000 bar, again in both crystallographic phases. Finally, shifts of the maximum of the $^1A_1 \rightarrow {}^1T_1$ absorption band during the thermal spin transition as well as during the relaxation process have been investigated.

[†] Universität Bern.
[‡] Université de Genève.
[⊗] Abstract published in *Advance ACS Abstracts,* November 15, 1997.

S1089-5647(97)02083-X CCC: $14.00

2. Experimental Section

2.1. Preparation of $[Zn_{1-x}Fe_x(ptz)_6](BF_4)_2$ and Crystal Growth. The mixed crystal series $[Zn_{1-x}Fe_x(ptz)_6](BF_4)_2$, $x = 0.1$, 0.32, and 1, was prepared using the procedure previously described.[12] Well-shaped single crystals were grown from nitromethane solutions by slow evaporation. The crystals are slightly bluish due to the tail of the $^5T_2 \rightarrow {}^5E$ absorption band extending from the infrared into the visible region and are formed as hexagonal plates up to several millimeters in diameter and about half a millimetre thick. The iron content was determined using the Lambert−Beer law and comparing the optical density of the $^1A_1 \rightarrow {}^1T_1$ band for the diluted compound with that of the concentrated compound.

2.2. Optical Spectroscopy and Pressure Experiments. Single-crystal absorption spectra in the region between 300 and 1300 nm were recorded on a Cary 5E spectrophotometer. For pressure experiments between 1 and 1000 bar single crystals of $[Zn_{1-x}Fe_x(ptz)_6](BF_4)_2$, $x = 0.1$, 0.32, and 1, were mounted inside the He-pressure cell described in ref 18. The cell was attached to the cold head of a closed-cycle refrigerator (Air-Products, Displex CSA-202) equipped with optical windows. Temperature control was realized using a PID temperature controller (Scientific Instruments), with a Si diode (Lake Shore DT-470) in thermal contact with the cell. Hydrostatic He-pressure of up to 1000 bar was achieved with a two-membrane pneumatic compressor (Novaswiss, Standard Type 554.3350).

In thermal equilibrium the high-spin fraction as a function of temperature and pressure, γ_{HS}, was calculated from the area under the $^1A_1 \rightarrow {}^1T_1$ absorption band between 430 and 670 nm relative to the area at 20 K, for which $\gamma_{HS} = 0$. The maximum of the $^1A_1 \rightarrow {}^1T_1$ band was determined using a Gaussian fit over a small interval around the band maximum.

Thermal transition curves were obtained using three different procedures. Procedure A: cooling down at ambient pressure from room temperature, applying pressure at low temperatures, and recording the spectra while warming up. Procedure B: applying the pressure at room temperature and recording the spectra during cooling down. Procedure C: applying the pressure at room temperature and cooling down under pressure, but then releasing the pressure at 20 K and collecting the spectra during warming up.

A quantitative population of the metastable high-spin state was achieved by irradiating the samples with 457 nm Ar^+ laser light at $T = 15$ K and a given pressure. Subsequently the temperature was raised to the desired value between 50 and 74 K, and the HS → LS relaxation was monitored by recording absorption spectra in the region of the $^1A_1 \rightarrow {}^1T_1$ band at fixed time intervals. HS → LS relaxation curves $\gamma_{HS}(t)$ were extracted from the area under this band relative to the area for $t \rightarrow \infty$.

3. Results and Discussion

3.1. The Thermal Spin Transition in $[Zn_{1-x}Fe_x(ptz)_6](BF_4)_2$. Figure 1a shows the thermal transition curves for $[Zn_{1-x}Fe_x(ptz)_6](BF_4)_2$, $x = 0.1$, at 1 bar and following procedures A, B, and C as described in section 2. The curve at 1 bar is gradual and fully reversible, as expected for a diluted system with noninteracting complexes, and it is in agreement with previous reports.[7,15] The curve obtained at 1000 bar following procedure A, that is, applying the pressure at 20 K after cooling down the sample at 1 bar, starts off gradual too, and it is shifted toward higher temperatures by about 28 K. This is expected on the basis of the work term $p\Delta V^{\circ}_{HL}$. At 115 K, however, there is a sudden drop in γ_{HS}. The subsequent transition curve is shifted toward higher temperatures by another 35 K, which is clearly too much to be due to the work term alone. The obvious

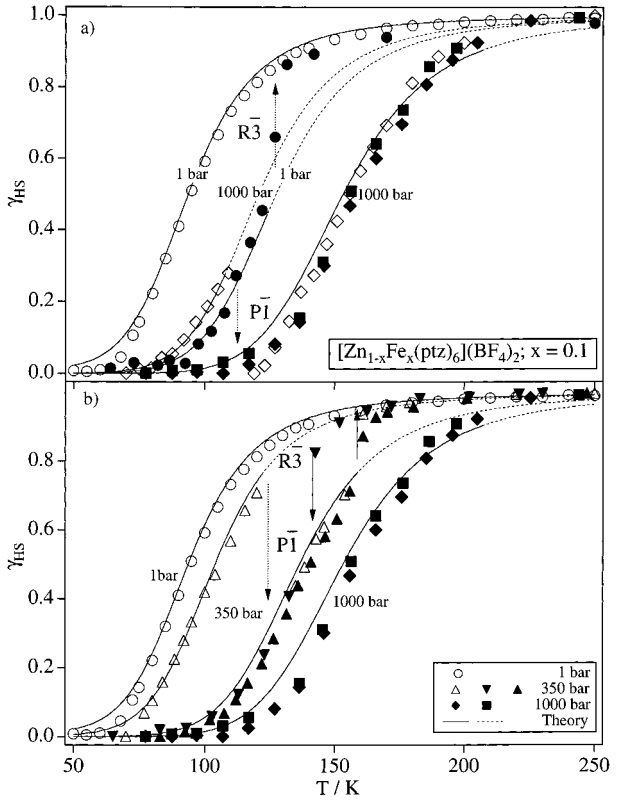

Figure 1. (a) Transition curves showing the high-spin fraction, γ_{HS}, as a function of temperature for a $[Zn_{1-x}Fe_x(ptz)_6](BF_4)_2$, $x = 0.1$, single crystal at pressures of 1 and 1000 bar and in the $R\bar{3}$ and $P\bar{1}$ crystallographic phases: 1 bar, $R\bar{3}$ (○), 1000 bar procedure A, $R\bar{3}$ and $P\bar{1}$ (◇), 1000 bar procedure B, $P\bar{1}$ (◆,■), 1 bar procedure C, $P\bar{1}$ and $R\bar{3}$ (●). (b) Transition curves in $[Zn_{1-x}Fe_x(ptz)_6](BF_4)_2$, $x = 0.1$, at pressures of 1 bar: (○), 350 bar: procedure A (Δ) and procedure B (▲,▼), and 1000 bar: (◆,■). The hysteresis induced with 350 bar external pressure is indicated by solid arrows. The relaxation of metastable phases is indicated by dotted arrows.

interpretation of this observation is that under pressure the $R\bar{3}$ phase is metastable at 20 K and that at 115 K it relaxes to its thermodynamically stable phase, with the most probable space group $P\bar{1}$.[19] That this is indeed the case is borne out by the transition curve at 1000 bar obtained following procedure B. It is once again gradual and fully reversible over the full temperature range, and it is identical to the previous curve above 115 K. Thus at 1000 bar the low-symmetry phase $P\bar{1}$ is the thermodynamically stable phase to above 200 K. At low temperatures the fourth curve in Figure 1a, obtained following procedure C, corresponds to the transition curve at 1 bar of the now metastable low-symmetry $P\bar{1}$ phase. Only at ∼121 K does the relaxation to the $R\bar{3}$ phase take place, and the transition curve subsequently continues along the very first curve of the series.

By choosing an intermediate pressure, it is possible to tune the crystallographic phase transition to occur at a temperature within the interval of the thermal spin transition. This is exemplified by the series of curves obtained at 350 bar shown in Figure 1b, following procedures A and B. The two reversible curves (i.e. $R\bar{3}$ at 1 bar and $P\bar{1}$ at 1000 bar) from Figure 1a are included as limiting curves. The curve at 350 bar following procedure A is now shifted toward higher temperatures by 11 K, and as before, the relaxation to the $P\bar{1}$ phase occurs at ∼120 K. In contrast to the curve at 1000 bar, the curves obtained following procedure B are not reversible any more. The crystallographic phase transition now occurs within the temperature interval of the spin transition, manifesting itself in a discontinuity in the spin transition and a thermal hysteresis with

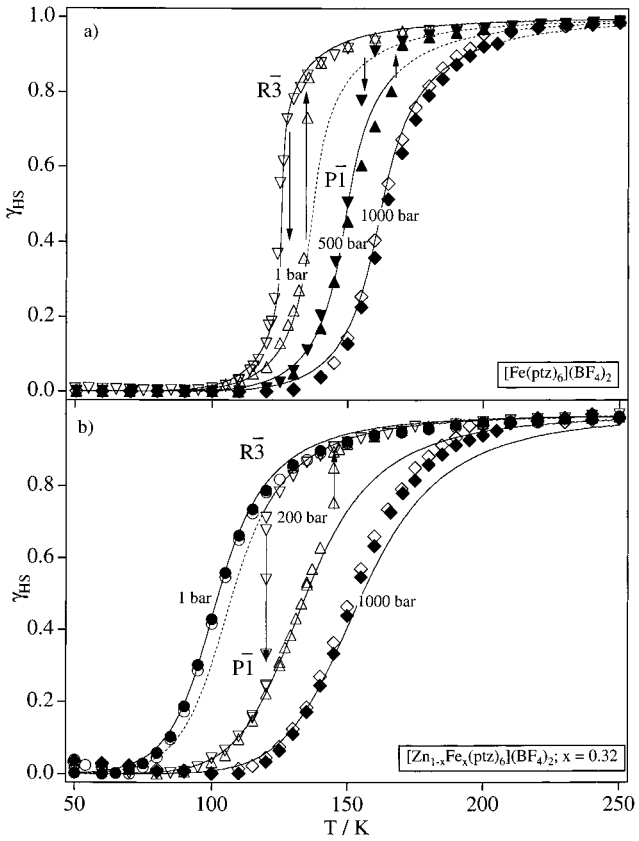

Figure 2. (a) Transition curves of the neat system $[Fe(ptz)_6](BF_4)_2$ at pressures of 1 bar (△,▽), 500 bar (▲,▼), and 1000 bar (◆,◇). The hysteresis due to the crystallographic phase transition $R\bar{3} \rightarrow P\bar{1}$ is indicated by solid arrows. (b) Transition curves of $[Zn_{1-x}Fe_x(ptz)_6](BF_4)_2$, $x = 0.32$. A hysteresis is induced with 200 bar external pressure.

$T_c^{\downarrow} = 140$ K and $T_c^{\uparrow} = 160$ K. However, within a given crystallographic phase the spin transition remains gradual.

The hysteresis behavior is a simultaneous function of p, x, and γ_{HS}, as shown in Figure 2a,b for $x = 1$ and $x = 0.32$, respectively. Figure 2a presents the transition curves in the neat system at ambient pressure and at elevated pressures of 500 and 1000 bar. The transition curve at ambient pressure obtained by cooling can have two different appearances, depending on how fast the cooling takes place. With fast enough cooling the crystallographic phase transition is suppressed, and the system remains in the $R\bar{3}$ phase, which is metastable at low temperatures.[14,15] For slow temperature variation the spin transition is accompanied by the above mentioned crystallographic phase transition from $R\bar{3}$ to $P\bar{1}$, with a thermal hysteresis of 7 K; that is, $T_c^{\downarrow} = 128$ K and $T_c^{\uparrow} = 135$ K, as previously reported.[12] In both crystallographic phases the transition curves are steep due to interactions between the spin-changing complexes in neat spin-crossover compounds. However, in both phases the interaction constant (see below) is not large enough to result in a hysteresis due to the interaction alone. The additional interplay with the crystallographic phase transition is needed. The transition curves for the neat system at 500 bar following procedure B, that is, cooling down under a given pressure, and afterwards warming up under the same pressure, show that with $T_c^{\downarrow} = 158$ K and $T_c^{\uparrow} = 168$ K the hysteresis is shifted to higher temperatures and has a slightly increased width compared to 1 bar. At the same time the jump in γ_{HS} at the discontinuity is substantially smaller. The 1000 bar curve is reversible up to 200 K and the system stays in the $P\bar{1}$ phase. Figure 2b shows the system with an iron content $x = 0.32$. As for $x = 0.1$, the transition curve at 1 bar is reversible, and the system remains in $R\bar{3}$ crystallographic phase over the full temperature range. But in contrast to $x = 0.1$, a pressure of only 200 bar is sufficient to induce the crystallographic phase transition with $T_c^{\downarrow} = 120$ K and $T_c^{\uparrow} = 145$ K. At 1000 bar the transition curves are again reversible, indicating that the system once more stays in the $P\bar{1}$ phase up to 200 K.

External as well as internal pressure induces the crystallographic phase transition because of the anisotropy of the crystal.[20] The influence of external pressure and the change in internal pressure, resulting from the spin transition, add up. In the neat system, the hysteresis is already present at ambient pressure because of the large contribution of the change in internal pressure. With an external pressure, an additional small change in internal pressure is sufficient to induce the $R\bar{3} \rightarrow P\bar{1}$ phase transition. Consequently, the phase transition takes place at higher values of γ_{HS} and with a smaller jump at the discontinuity. At the same time the hysteresis becomes broader, because it occurs in the part of the transition curve which is flatter. In the system with lower iron fractions, $x = 0.1$ and 0.32, the transition curves at 1 bar are reversible. They remain so to approximately 300 bar for the former and to 150 bar for the latter. For $x = 0.1$, the interaction between the spin-changing complexes is small, but for $x = 0.32$ it is not negligible, and the additional pressure needed to induce the crystallographic phase transition is smaller.

The fact that the width of the hysteresis is a function of x, that is 7 K for $x = 1$ and 1 bar compared to 25 K for $x = 0.32$ at 200 bar, can also be rationalized qualitatively. The difference in internal pressure between $T_c^{\downarrow}$ and $T_c^{\uparrow}$ in a given phase has to be more or less independent of x. For the larger concentration a smaller difference in γ_{HS} already results in the required change in internal pressure, and hence the width of the hysteresis in the concentrated system is smaller. This explanation is corroborated by the observation that in the full mixed crystal series of the title compound $x\gamma_{LS}(T_c^{\downarrow}) \approx 0.22$ for all values of x. Thus the $R\bar{3} \rightarrow P\bar{1}$ transition occurs at approximately equal values of the internal pressure.[15]

To compare the position of the transition curves quantitatively, the transition temperature $T_{1/2}$, defined as the temperature for which $\gamma_{HS} = 0.5$, as a function of pressure is shown in Figure 3. In a given crystallographic phase and for a given dilution, $T_{1/2}$ increases linearly with pressure. Within experimental error, and with one exception, almost the same slopes between 27(2) and 30(2) K/kbar are obtained. Thus the influence of the external pressure on the system is similar in both crystallographic phases. The somewhat smaller slope for the system with $x = 0.32$ in the $P\bar{1}$ phase of 23(1) K/kbar could be due to a slightly different order in the crystal packing or a higher degree of disorder in the stacking sequence along the c-axis compared to the neat iron system or the system containing a majority of zinc complexes.

In the inset of Figure 3, the shift of $T_{1/2}$ due to the crystallographic phase transition at ambient pressure is shown. In the diluted systems of $x = 0.1$ and $x = 0.32$ the shift is 32 and 26 K, respectively, whereas in the neat system it is 11 K. The substantial decrease, proportional to the amount of iron(II) complexes, is attributed to the cooperative effects and to the distinctly different interaction constants in the two crystallographic phases (vide infra).

3.2. Determination of the Thermodynamic Parameters. The Gibbs free energy of a neat spin-crossover system in a given crystallographic phase and containing a random distribution of γ_{HS} complexes in the HS state and $\gamma_{LS} = 1 - \gamma_{HS}$ complexes in the LS state, considering the iron fraction x in an inert host lattice, can be written as[3]

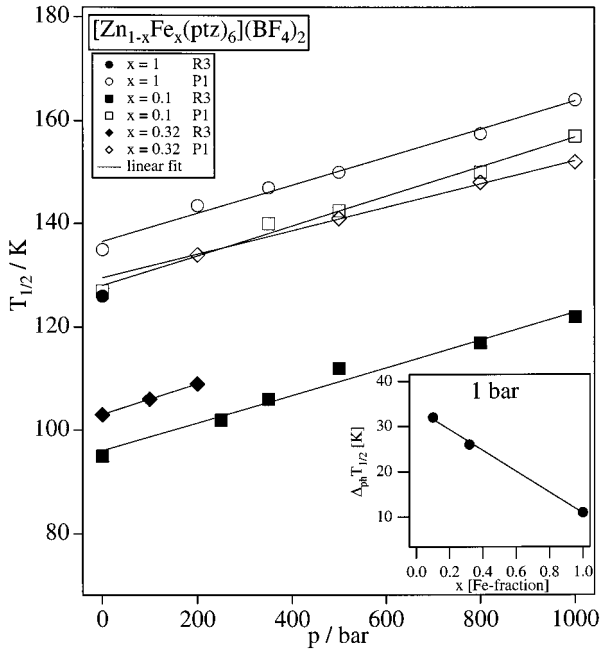

Figure 3. Shifts of a transition curve measured at the transition temperature $T_{1/2}$ in a given crystallographic phase and for a given dilution toward higher temperatures as a function of an external pressure. Inset: Dependence of the $T_{1/2}$ shift between the two crystallographic phases on the iron fraction.

$$G(\gamma_{HS},x,p,T) = x\gamma_{HS}\,(\Delta F_{HL}^{x\to 0}(T) + p\Delta V_{HL}^{\circ}) - TS_{mix}(\gamma_{HS}) + G^{int}(\gamma_{HS},x,p,T) \quad (1)$$

where all γ_{HS} independent terms have been omitted. $\Delta F_{HL}^{x\to 0}(T) = F_{HS}^{x\to 0}(T) - F_{LS}^{x\to 0}(T)$ corresponds to the free energy difference between the HS and the LS state in a given reference lattice and can, for instance, be determined from transition curves obtained for highly diluted mixed crystals, with the iron(II) complex doped into an isomorphous host lattice. Jung et al.[43,44] did this for the $R\bar{3}$ phase of $[Zn_{1-x}Fe_x(ptz)_6](BF_4)_2$, $x = 0.005$, and parametrized it as $\Delta F_{HL}^{x\to 0,R\bar{3}}(T) = A - BT + CT^2$, $A = 758\ cm^{-1}$, $B = 6.31\ cm^{-1}\ K^{-1}$, $C = 17\,100\ cm^{-1}\ K^2$. $S_{mix} = -xk_B[\gamma_{HS}\ln\gamma_{HS} + (1-\gamma_{HS})\ln(1-\gamma_{HS})]$ is the mixing entropy, and $\Delta V_{HL}^{\circ} = V_{HS} - V_{LS}$ is the difference in volume between the two states. G^{int} accounts for all interactions between the spin-changing molecules. In mean-field approximation it can be expanded in the form[3,21]

$$G^{int}(\gamma_{HS},x) = x^2\gamma_{HS}\Delta - x^2{\gamma_{HS}}^2\Gamma \quad (2)$$

The interaction constant Γ describes the interaction between HS and LS complexes, and the lattice shift Δ depends upon their interaction with the reference lattice. In the following, the temperature dependence of Δ and Γ are assumed to be negligible.[52]

The condition for thermal equilibrium

$$\left(\frac{\partial G}{\partial \gamma_{HS}}\right)_{T,p} = 0 \quad (3)$$

results in the implicit equation of state

$$\Delta F_{HL}^{x\to 0}(T) + x\Delta - 2x\Gamma\gamma_{HS} + p\Delta V_{HL}^{\circ} + k_B T \ln\frac{\gamma_{HS}}{1-\gamma_{HS}} = 0 \quad (4)$$

A simultaneous least-squares fit to the transition curves of $[Zn_{1-x}Fe_x(ptz)_6](BF_4)_2$ in the $R\bar{3}$ phase, $x = 0.1$, 0.32, and 1, given in Figures 1 and 2, plus the full series of transition curves at various pressures between 1 and 1000 bar not explicitly shown, gave values for ΔV_{HL}°, Γ, and Δ of 26(3) Å^3, 170(9) cm^{-1}, and 340(9) cm^{-1}, respectively (see Table 1). These are in good agreement with values previously reported using a stepwise evaluation procedure[7] and with those given by Jung et al.[15] based on a very sophisticated treatment of the interaction constant including a discussion of its temperature dependence.

TABLE 1: Thermodynamic Parameters, Relaxation Rate Constants, Self-Acceleration Factors, and Acceleration Factors Due to External Pressure of the Two Crystallographic Phases of $[Zn_{1-x}Fe_x(ptz)_6](BF_4)_2$, $x = 0.1$, 0.32, and 1, and of $[Fe(ptz)_6](PF_6)_2$ from Ref 8[a]

compound	$[Zn_{1-x}Fe_x(ptz)_6](BF_4)_2$		$[Fe(ptz)_6](PF_6)_2$
cryst. phase	$R\bar{3}$	$P\bar{1}$	$P\bar{1}$
ΔV_{HL}° [Å^3]	26(4)	29(4)	24(2)
Γ [cm^{-1}]	170(9)	144(8)	101(5)
Δ, $\Delta+\theta_1$ [cm^{-1}]	340(9)	204(8)	
θ_0 [cm^{-1}]		176(8)	
k_{HL}°, 1 bar [s^{-1}]	$\leq 10^{-6}$	$\approx 5\times 10^{-5}$	$\leq 5\times 10^{-7}$
$\alpha(T\to 0)$	5	1	2
$\beta(T\to 0)$ [kbar^{-1}]	2.6	2.8	2.8
$\Gamma/\Delta V_{HL}^{\circ}$ [kbar]	1.31	0.99	0.84

[a] $\Delta V_{HL}^{\circ} = V_{HS} - V_{LS}$: difference in volume between complexes in the HS state and complexes in the LS state. Γ: interaction constant; Δ, $\Delta+\theta_1$: lattice shift due to the interaction between spin-changing molecules and and the host lattice. θ_0: energy shift due to the crystallographic phase transition. $k_{HL}^{\circ}(T\to 0)$: low-temperature tunneling rate constant at zero external pressure and $\gamma_{LS} = 0$, respectively. α: acceleration factor due to cooperative effects. β: acceleration factor due to external pressure.

For the $P\bar{1}$ phase, $\Delta F_{HL}^{x\to 0}(T)$ is a priori not known, because it is not possible to record a full transition curve at 1 bar of the very diluted system. However, assuming that the reaction entropy is given by the electronic structure and local vibrations, $\Delta F_{HL}^{x\to 0}(T)$ of the low-symmetry phase differs from $\Delta F_{HL}^{x\to 0}(T)$ of the high-symmetry phase only by an x-dependent energy shift according to

$$\Delta F_{HL}^{x\to 0,P\bar{1}} \approx \Delta F_{HL}^{x\to 0,R\bar{3}} + \theta(x) \quad (5)$$

Furthermore, the inset of Figure 3 shows that the shift in $T_{1/2}$ from the high to the low-symmetry phase decreases monotonously with x, from 35 K at $x = 0.1$ to 11 K for $x = 1$. In a linear approximation $\theta(x)$ may thus be expanded as

$$\theta(x) = \theta_0 + \theta_1 x \quad (6)$$

A simultaneous least-squares fit to all transition curves for $[Zn_{1-x}Fe_x(ptz)_6](BF_4)_2$, $x = 0.1$, 0.32, and 1, with ΔV_{HL}°, Γ, θ_0, and $(\theta_1+\Delta)$ as free parameters, gave values of 29(4) Å^3, 144(8) cm^{-1}, 176(8) cm^{-1}, and 204(8) cm^{-1}, respectively. θ_1 and Δ, both being linear in x, cannot be separated without further model assumptions. The value for ΔV_{HL}° is in fair agreement with the value of approximately 35 Å^3 from the independent X-ray experiment.[19]

The thermodynamic parameters determined for the $[Zn_{1-x}Fe_x(ptz)_6](BF_4)_2$ mixed crystal system are given in Table 1, together with those for the related $[Fe(ptz)_6](PF_6)_2$. In Figures 1 and 2, calculated transition curves using these parameters are shown. They match the experimental data satisfactorily for all concentrations and pressures and in both crystallographic phases. Compared to the $R\bar{3}$ phase, the interaction constant for the $P\bar{1}$ phase is smaller, but the volume difference is larger. There is no obvious correlation between Γ and ΔV_{HL}°. The phenomenological interaction constant is made up of various contributions: isotropic contributions, which are directly related to ΔV_{HL}° and which are always positive, and anisotropic contri-

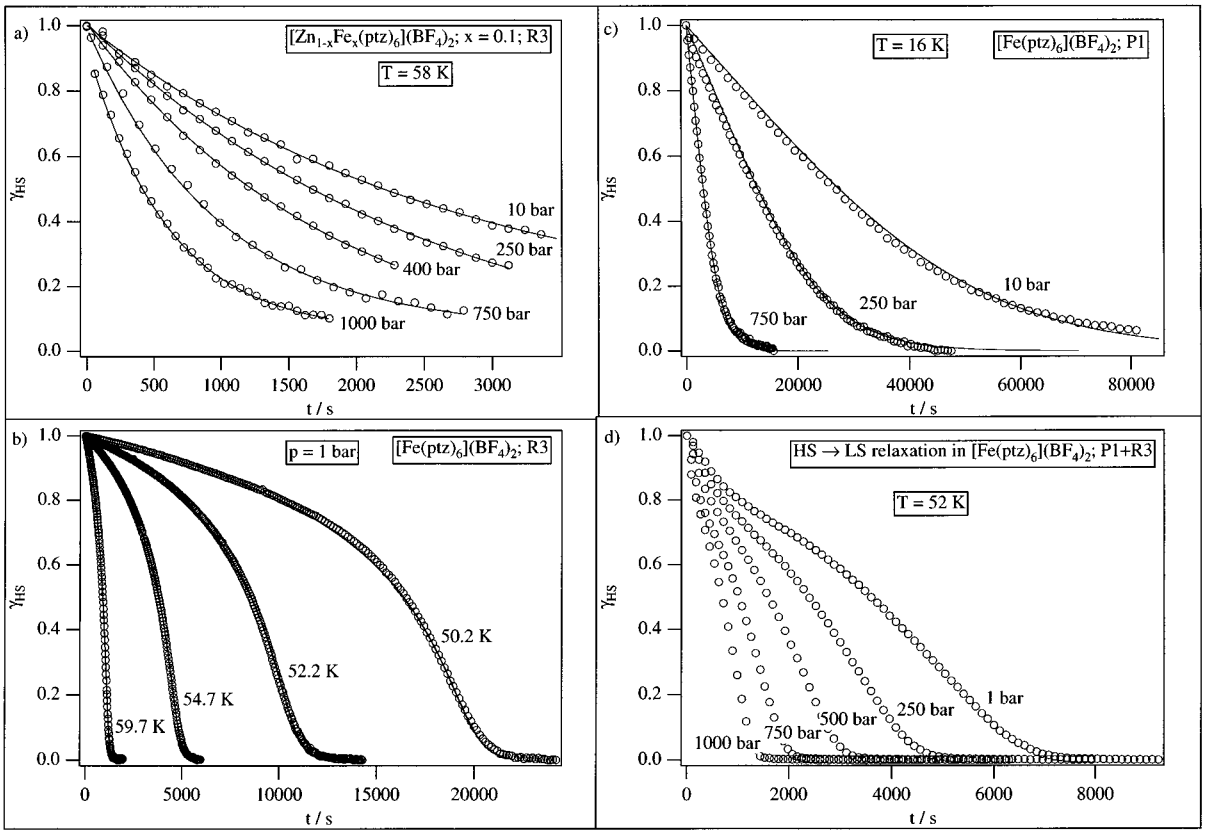

Figure 4. HS → LS relaxation curves of (a) $[Zn_{1-x}Fe_x(ptz)_6](BF_4)_2$, $x = 0.1$ in the $R\bar{3}$ phase at $T = 58$ K and $p = 10$, 250, 400, 750, and 1000 bar; (b) $[Fe(ptz)_6](BF_4)_2$ in $R\bar{3}$ phase at $p = 1$ bar and $T = 50.2$, 52.2, 54.7, and 59.7 K (adapted from ref 40); (c) $[Fe(ptz)_6](BF_4)_2$ in $P\bar{1}$ phase at $T = 16$ K and $p = 10$, 250, and 750 bar; (d) $[Fe(ptz)_6](BF_4)_2$ in a mixture of $R\bar{3}$ and $P\bar{1}$ phases at $T = 52$ K and $p = 1$, 250, 500, 750, and 1000 bar.

butions, which can have either sign.[15,20] Thus a larger negative contribution in the low-symmetry phase may result in a smaller overall value for Γ despite the larger value of ΔV°_{HL}.

3.3. The HS → LS Relaxation. The HS → LS relaxation in $[Zn_{1-x}Fe_x(ptz)_6](BF_4)_2$, $x = 0.1$, in both crystallographic phases is a single-exponential function following the kinetics of a first-order reaction, as for example shown in Figure 4a at 58 K in the $R\bar{3}$ phase. Under the influence of external pressure, the relaxation is still single exponential but accelerated compared to ambient pressure. The corresponding HS → LS relaxation rate constants, $k_{HL}(p,T)$, as a function of temperature at 1 bar and 1000 bar are shown in form of an Arrhenius plot in Figure 5a. Two regions with different relaxation mechanisms can be distinguished: the classical region and the tunnelling region. In the classical region at temperatures above ~80 K the relaxation is thermally activated, with an experimental activation energy ΔE^{a}_{HL} of 1185(18) cm^{-1}.[11,16] In the tunnelling region at temperatures below ~40 K, the relaxation is temperature independent and levels off toward a limiting value for the rate constant $k_{HL}(T \rightarrow 0) \leq 10^{-6}$ s^{-1}. At low temperatures external pressure accelerates the relaxation by about 1 order of magnitude per kbar.

The relaxation in the $P\bar{1}$ phase in the diluted system is still single exponential but it proceeds faster than in the $R\bar{3}$ phase. It can therefore be followed to lower temperatures. The corresponding rate constants down to 16 K are included in Figure 5a, with $k_{HL}(T \rightarrow 0) \approx 5 \times 10^{-5}$ s^{-1}. The values at 1000 bar are included as well, and again an acceleration of about 1 order of magnitude is observed. The acceleration due to external pressure is exponential according to

$$k_{HL}(p,T) = k_{HL}(p \rightarrow 0,T) \exp(\beta p) = k^{\circ}_{HL}(T) \exp(\beta p) \quad (7)$$

The acceleration factor β, obtained as the slope in the plot of $\ln[k_{HL}(p)/k^{\circ}_{HL}]$ versus pressure at a given temperature, is shown in Figure 5b as a function of temperature for the mixed system in both crystallographic phases.

The temperature dependence of the HS → LS relaxation in $[Fe(ptz)_6](BF_4)_2$ in the $R\bar{3}$ phase has been previously investigated.[17] The corresponding relaxation curves are reproduced in Figure 4b. The strong deviation from first-order kinetics due to cooperative effects are obvious. Spectroscopic evidence (vide infra) show that it is the change in vertical displacement of the two potential wells relative to each other as a function of internal pressure that is mainly responsible for the observed self-acceleration. The kinetics of the self-accelerated reaction is described phenomenologically by a relaxation rate constant depending upon the LS fraction according to

$$k_{HL}(\gamma_{LS},T) = k_{HL}(\gamma_{LS}=0,T) \exp(\alpha\gamma_{LS}) = k^{\circ}_{HL}(T) \exp(\alpha\gamma_{LS}) \quad (8)$$

that is, an exponential increase with increasing LS fraction. The initial rate constants, k°_{HL}, for the neat compound as well as the final rate constants, $k^{\circ}_{HL}\exp(\alpha\gamma_{LS})$, obtained after partial light-induced conversion to the HS state, are included in the Arrhenius plot of Figure 5a. The self-acceleration factor α for $[Fe(ptz)_6](BF_4)_2$ in the $R\bar{3}$ phase is shown in Figure 5b.

A peculiar feature of the neat compound is that in its $P\bar{1}$ phase the relaxation proceeds almost single exponentially (see Figure 4c). The acceleration factor α is only ~1 and almost temperature independent in the temperature range between 16 and 46 K. The acceleration by the external pressure, however, is again exponential with $\beta(T \rightarrow 0) \approx 2.7$. The values of β in the $P\bar{1}$ phase are included in Figure 5b.

Unfortunately, cooling down in the He-pressure cell is not fast enough for a crystal of the neat compound to remain

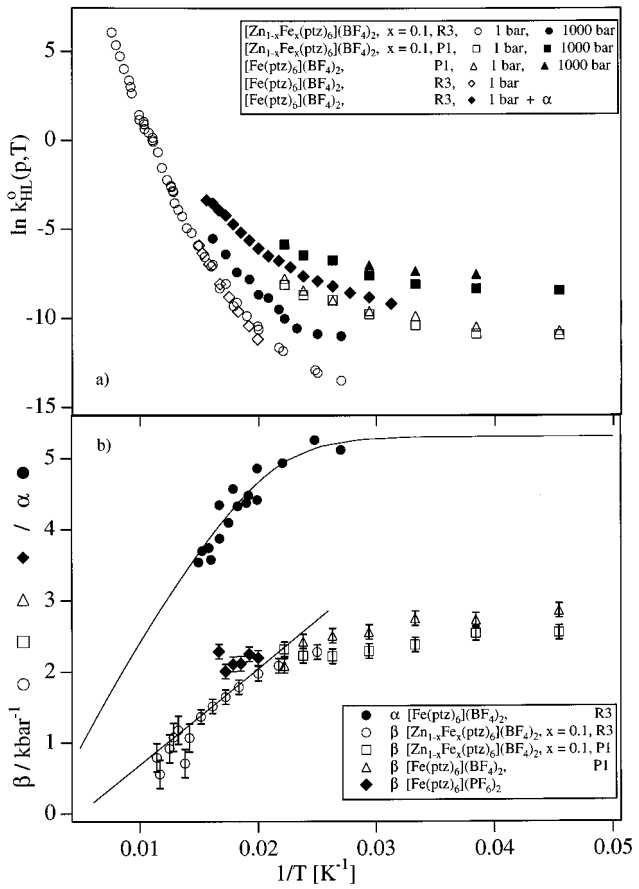

Figure 5. (a) Arrhenius plot of the rate constant, ln[k] vs 1/T, as functions of temperature for $[Zn_{1-x}Fe_x(ptz)_6](BF_4)_2$, $x = 0.1$, and initial and final rate constants for $[Fe(ptz)_6](BF_4)_2$ in crystallographic phases $R\bar{3}$ and $P\bar{1}$. (b) Self-acceleration factor α for $[Fe(ptz)_6](BF_4)_2$ in the $R\bar{3}$ phase. Acceleration factor $\beta(T)$ due to the external pressure as a function of inverse temperature for $[Zn_{1-x}Fe_x(ptz)_6](BF_4)_2$, $x = 0.1$ and 1, in both crystallographic phases and for $[Fe(ptz)_6](PF_6)_2$.

completely in the $R\bar{3}$ phase. This can be deduced from the shape of the relaxation curves in Figure 4d, where a combination of the two typical shapes can be seen: the quasi-exponential one and the sigmoidal one, indicating that a mixture of two crystallographic phases is present in the crystal. Complexes in the $P\bar{1}$ phase relax faster at a given pressure and temperature compared to those in the $R\bar{3}$ phase, but a quantitative evaluation of individual rate constants is still not straightforward.

The interdependence of external and internal pressure in the related $[Fe(ptz)_6](PF_6)_2$ system, for which there is no crystallographic phase transition, has been studied previously.[8] The self-acceleration factor α of ∼2 in $[Fe(ptz)_6](PF_6)_2$ is substantially smaller than the corresponding low-temperature value of ∼5 in the $R\bar{3}$ phase of $[Fe(ptz)_6](BF_4)_2$, but larger than the value of ∼1 in the $P\bar{1}$ phase. In contrast, values of the acceleration factor β in the PF_6 system lie close to the common curve for the title system (see Figure 5b). For $[Fe(ptz)_6](PF_6)_2$, it has been shown that within experimental error the self-acceleration does not depend on the external pressure and that the effects of internal and external pressure add up according to[8]

$$k_{HL}(\gamma_{LS},p,T) = k^{\circ}_{HL}(T)\exp(\alpha\gamma_{LS} + \beta p) \qquad (9)$$

In the tetrazole systems investigated so far, with their characteristic layer structure, β follows a similar temperature dependence. At higher temperatures, the relation $\beta = -\Delta V^{\#}_{HL}/k_BT$ holds, with a resulting value of the activation volume $\Delta V^{\#}_{HL} \approx -17$ Å^3. The activation volume is somewhat larger in absolute terms than $\Delta V^{\circ}_{HL}/2$. In the tunnelling region, β becomes temperature independent and is a function of the Huang−Rhys factor, S, and the reduced energy gap, n.[23] The Huang−Rhys factor accounts for the horizontal displacement of the potential wells relative to each other, and the reduced energy gap is a measure of the vertical displacement. Both of these factors are normalized to the vibrational quanta $\hbar\omega$, which for iron(II) spin-crossover compounds are typically around 250 cm^{-1}.[24] They are defined as $S = (1/2)f\Delta Q_{HL}^2/\hbar\omega$ and $n = \Delta E^{\circ}_{HL}/\hbar\omega$, where ΔQ_{HL} is the displacement between the HS and LS state along the totally symmetric vibrational coordinate, and ΔE°_{HL} is the zero-point energy difference. In terms of the two parameters the low-temperature tunnelling rate constant is given by the proportionality[25]

$$k_{HL}(T\rightarrow 0) \sim \frac{S^n e^{-s}}{n!} \qquad (10)$$

For iron(II) spin-crossover compounds a value of S of ∼45 has been estimated,[26] and n is on the order of 1. With $S \gg n \approx 1$, that is in the strong vibronic coupling limit,[40]

$$k_{HL}(T\rightarrow 0) \sim S^n e^{-S} = e^{(\ln S)n - S} \qquad (11)$$

An internal pressure and an external pressure change both Δr_{HL} and ΔE°_{HL}. The influence of pressure on the horizontal displacement of the potential wells can be expressed as

$$S(p) = S(p\rightarrow 0) + \Delta S = S(p\rightarrow 0) + \beta_S p \qquad (12)$$

while the vertical displacement under pressure is

$$n(p) = n(p\rightarrow 0) + \Delta n = n(p\rightarrow 0) + \beta_n p \qquad (13)$$

β_S accounts for the change in Δr_{HL} of around 10^{-3} Å/kbar [11] and is given by the expression

$$\beta_S \approx 2S\left(\frac{\delta\Delta r_{HL}}{\Delta r_{HL}}\right) \approx -0.5\ \text{kbar}^{-1} \qquad (14)$$

β_n accounts for the increase in ΔE°_{HL} due to the work term $p\Delta V^{\circ}_{HL}$. With the value of ΔV°_{HL} for the diluted system in the $R\bar{3}$ phase of 26 Å^3, the latter takes on a value of 130 cm^{-1} kbar^{-1}, resulting in the relation

$$\beta_n \approx \frac{\Delta V^{\circ}_{HL}}{\hbar\omega} \approx 0.5\ \text{kbar}^{-1} \qquad (15)$$

The horizontal change is distinctly smaller than the vertical one, and the low-temperature tunnelling rate constant as a function of pressure can now be written as[8]

$$k_{HL}(T\rightarrow 0,p) = k^{\circ}_{HL}(T\rightarrow 0,p\rightarrow 0)e^{[(\ln S)\beta_n - \beta_S]p} \qquad (16)$$

The total acceleration factor in the tunnelling region is then given by

$$\beta(T\rightarrow 0) \approx (\ln S)\beta_n - \beta_S \qquad (17)$$

With the above mentioned values, $\beta(T\rightarrow 0) \approx 2.5$ kbar^{-1} can been estimated, which is in good agreement with the experimental value of ∼2.7 kbar^{-1}.

The interpretation of eq 8 for the rate constant as a function of γ_{LS} in the neat compound is straightforward. The elastic interactions are well described by an internal pressure modulating ΔE°_{HL} linearly with γ_{LS}. Based on the comparison of the low-temperature values of the self-acceleration factor α and the

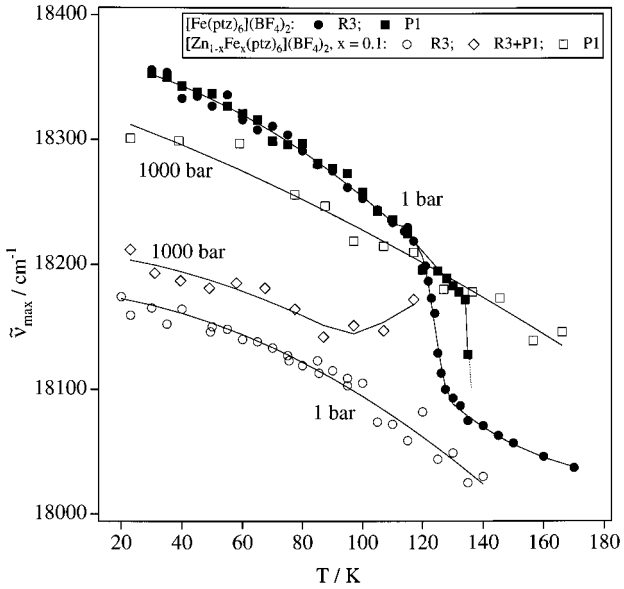

Figure 6. Energy shifts of the $^1A_1 \rightarrow {}^1T_1$ band maximum during the spin transition as a function of temperature in $[Zn_{1-x}Fe_x(ptz)_6](BF_4)_2$, $x = 0.1$ and 1, for both crystallographic phases and at pressures of 1 and 1000 bar.

pressure factor β in the $R\bar{3}$ phase of 5.2 and 2.7, respectively, the difference in internal pressure between $\gamma_{LS} = 1$ and $\gamma_{LS} = 0$ corresponds to an external pressure of approximately 2 kbar. Thus the increase in ΔE°_{HL} in the neat compound during the relaxation is $\sim$260 cm^{-1}. This increase is related to the interaction constant Γ used to describe the thermal spin transition. Within the isotropic model it should be equal to 2Γ. For the highly symmetric $R\bar{3}$ phase with $\Gamma = 170$ cm^{-1}, the two values are in reasonable agreement with each other. In the $P\bar{1}$ phase, on the other hand, the value for $\alpha(T \rightarrow 0)$ is substantially smaller than expected from the corresponding value for Γ.

3.4. The Shift of the $^1A_1 \rightarrow {}^1T_1$ Band Maximum. The energy shift of the $^1A_1 \rightarrow {}^1T_1$ band maximum is a simultaneous function of pressure, temperature and LS fraction. Figure 6 shows the shifts in the title system as a function of temperature for $x = 0.1$ and 1, for both crystallographic phases and at pressures of 1 and 1000 bar. The curve at the lowest energy is that of the diluted system at 1 bar in the $R\bar{3}$ phase. The energy of the band maximum decreases monotonously by 150 cm^{-1} between 20 and 140 K due to the thermal expansion of the lattice.

External pressure shifts the band maximum toward higher energies. For the diluted system in the $R\bar{3}$ phase, the shift is linear in pressure up to 2000 bar (see Figure 7) with a slope $\Delta\nu_p \approx 85$ cm^{-1} kbar^{-1}. This, in turn, is due to a small but significant decrease in metal−ligand bond length of the LS state with increasing pressure, as a result of which the ligand-field strength of the LS species, $10Dq^{LS}$, increases according to[27]

$$10Dq^{LS} \approx r_{LS}^{-6} \qquad (18)$$

With increasing temperature, the second curve in Figure 6, initially corresponding to the band maximum at 1000 bar in the metastable $R\bar{3}$ phase, runs parallel to the curve at 1 bar up to a temperature of $\sim$100 K, where the relaxation to the $P\bar{1}$ phase takes place. As a result, the band maximum shifts to the third curve, which corresponds to the band maximum of the diluted system in the $P\bar{1}$ phase. This curve, too, runs parallel to the first curve but displaced toward higher energies by another 100 cm^{-1} with respect to the second curve. This difference is solely due to the crystallographic phase transition.

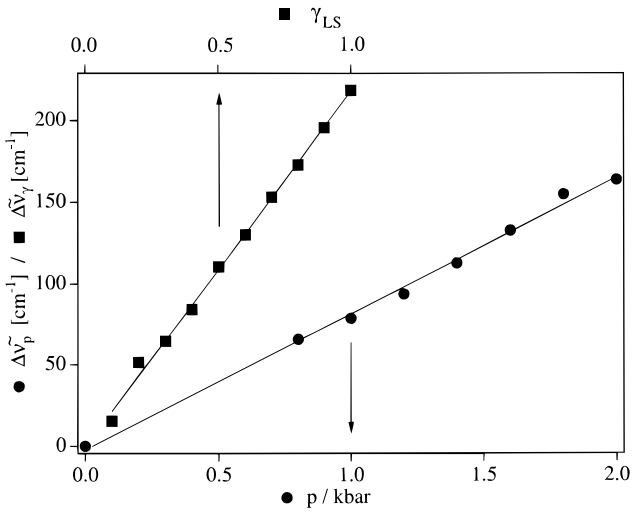

Figure 7. Energy shift of the $^1A_1 \rightarrow {}^1T_1$ band maximum as a function of the external pressure $\Delta\tilde{\nu}_p$ (●) at 44 K, and the low-spin fraction $\Delta\tilde{\nu}_\gamma$ (■) at 57 K.

The fourth curve in Figure 6 shows the energies of the band maximum for the neat system in the two different crystallographic phases. Compared to the diluted system in the $R\bar{3}$ phase, the energy of the band maximum in the neat system is about 200 cm^{-1} higher at 20 K. The shift of the band maximum follows the abrupt behaviour of the transition curve and the energy of the band maximum decreases with decreasing low-spin fraction. The values for the two phases in the neat system follow the same curve up to the spin transition where the hysteresis behaviour is reflected. The contribution to the shift across the thermal spin transition due to cooperative effects is approximately 160 cm^{-1}.

The above shifts of the $^1A_1 \rightarrow {}^1T_1$ absorption band can be qualitatively related to changes in the zero-point energy difference between the HS and the LS state ΔE°_{HL}. According to the Tanabe−Sugano diagram for a d^6 system,[28] the shift in the maximum of the $^1A_1 \rightarrow {}^1T_1$ absorption band is equal to the change in ligand-field strength of the LS species, $\delta 10Dq^{LS}$, and according to Clack and Smith,[29] ΔE°_{HL} is a linear function of $10Dq^{LS}$ with slope 1. Thus the shift with external pressure, $\Delta\nu_p$, should in turn be equal to the contribution of the work term $p\Delta V^\circ_{HL}$ to ΔE°_{HL}. The above mentioned value of 130 cm^{-1} is somewhat larger than the value of 85 cm^{-1} kbar^{-1} for $\Delta\nu_p$, but considering the actual complexity of the problem, the two values are in reasonable agreement.

For the neat system, the increase in energy with increasing LS fraction can also be discussed on the basis of Figure 7, where the shift of the band maximum during the HS → LS relaxation in the $R\bar{3}$ phase at a constant temperature of 57 K is shown. With 220 cm^{-1} the total shift is close to the value for the change in ΔE°_{HL} derived from the acceleration parameter $\alpha(T \rightarrow 0)$. A comparison of the two curves in Figure 7 supports the above statement that 2 kbar external have a roughly equal effect as the difference in internal pressure between $\gamma_{LS} = 1$ and $\gamma_{LS} = 0$.

4. Conclusions

The study of both the spin equilibrium and the HS → LS relaxation under external pressure in the mixed crystal series $[Zn_{1-x}Fe_x(ptz)_6](BF_4)_2$, $x = 0.1$, 0.32, and 1, provides the basis of a quantitative determination of thermodynamic and kinetic parameters and gives insight into their interdependence. In contrast to the $[Fe(ptz)_6](PF_6)_2$ system, which is in the $P\bar{1}$ phase at all pressures and temperatures,[28] the crystallographic phase

transition from $R\bar{3}$ at ambient temperatures to $P\bar{1}$ at cryogenic temperatures observed in the title compound adds the challenging task of a simultaneous explanation of all the observed phenomena associated with the spin transition, in particular the hysteresis behaviour. Because of the comparatively high symmetry of the title compound and in the absence of any anomalies in the transition curves, a mean-field approach in which long range interactions are averaged over the whole crystal proved to be adequate. From the simultaneous fit to all $\gamma_{HS}(T,p,x)$ curves in a given crystallographic phase, two sets of physical parameters have been determined, that is, the volume difference between the HS and the LS state, ΔV°_{HL}, the interaction constant describing interactions between spin changing molecules Γ, the energy shift due to the phase transition as a function of iron fraction $\theta(x)$, and finally the lattice shift Δ coming from the interactions of spin-changing molecules with the reference lattice.

The observed hysteresis in the spin transition of the neat compound at ambient pressure is due to the crystallographic phase transition and not to the elastic interaction as such. Of course, the elastic interactions trigger the phase transition, but the values of the interaction constants in either phase are not large enough to result in a hysteresis on their own. The transition curves in either phase are quite steep but reversible. The values of the so-called reduced pressure Π^*, relating the total energy separation between the HS and LS state $\Delta F^{\circ}_{HL}(T) + \Delta + p\Delta V^{\circ}_{HL}$ to the interaction energy Γ,[30] for the $R\bar{3}$ and the $P\bar{1}$ phase at $p = 1$ bar and at the critical temperature $T_{crit} = \Gamma/k_B T$, are approximately 2 and 3, respectively. Only for values of Π^* less than 1 is the spin transition itself expected to occur as a first-order phase transition.

The ratio $\Gamma/\Delta V^{\circ}_{HL}$ has the physical dimensions of pressure. In the isotropic model it should be equal to the difference in internal pressure between $\gamma_{LS} = 1$ and $\gamma_{LS} = 0.5$, and, in principle, it should be amenable to a direct comparison with the effects of an external pressure. For the neat system in the $R\bar{3}$ phase, $\Gamma/\Delta V^{\circ}_{HL} = 1.3$ kbar, and indeed, an external pressure of 1.3 kbar is extrapolated to shift the transition temperature by 36 K (see Figure 3), which is close to the difference in transition temperature of 34 K between the highly diluted system, $x = 0.005$ with $T_{1/2} = 91$ K,[15] and the neat system.

The concept of an internal pressure is only valid as limiting case for isotropic systems with dominant long-range interactions. Thus the comparison of the effects of an external pressure with those of the elastic interaction works quite well for the title system in the high-symmetry phase. Shifts of transition curves, shifts of absorption bands, and the acceleration of the HS $\rightarrow$ LS due to internal and external pressure can all be explained consistently at least semiquantitatively. For the low-symmetry phase, however, a quantitative comparison of thermodynamic, kinetic, and spectroscopic parameters as well as a cross-reference to the parameters of the high-symmetry phase are not possible. The higher anisotropy of the system in the low-symmetry phase reduces the interaction constant, despite the larger value of ΔV°_{HL} compared to the high-symmetry phase. This reduction is not too large, however, the concomitant dramatic reduction of the self-acceleration factor α is puzzling. At this stage, the reasons for this discrepancy are not clear. It could be due to specific nearest neighbor interactions, leading to nonrandom distributions of HS and LS complexes during the relaxation. Of course, in order to account for such interactions, the mean-field approach adopted here is not sufficient.

The relevant quantity for the HS $\rightarrow$ LS relaxation is ΔE°_{HL}, that is, zero-point energy difference between the ground state and the lowest energy component of the HS manifold. For the spin equilibrium the relevant quantity is ΔG°_{HL}, which contains a thermal average over the HS manifold. If a perturbation, be it external pressure or elastic interactions, influences the splitting of the HS manifold, then its effect on the relaxation will be different from its effect on the equilibrium. Particularly in the low-symmetry system, both, external pressure as well as elastic interactions, will give rise to non-totally symmetric distortions, as a result of which the quantitative aspect of the relation between kinetic, spectroscopic, and thermodynamic parameters is lost. Additionally, the distortions due to an external pressure may be different from those due to the elastic interactions.

Acknowledgment. We thank R. Jakobi and H. Spiering for access to valuable results prior to publication. R. Hinek, H. Weihe, and H. Romstedt are acknowledged for helpful discussions, F. Varret for useful comments, U. Kindler for building the pressure cell, and H. U. Güdel for the use of equipment. This work was supported by the "Schweizerischer Nationalfonds" and the "Hochschulstiftung der Universität Bern".

References and Notes

(1) (a) Gütlich, P. *Struct. Bonding* **1981**, *44*, 83. (b) König, E *Progr. Inorg. Chem.* **1987**, *35*, 527. (c) Gütlich, P.; Hauser, A.; Spiering, H. *Angew. Chem. Int. Ed. Engl.* **1994**, *33*, 2024.

(2) Kahn, O. *Curr. Opin. Solid State Mater. Sci.* **1996**, *1*, 547.

(3) (a) Slichter, C. P.; Drickamer, H. G. *J. Chem. Phys.* **1972**, *56*, 2142. (b) Drickamer, H. G.; Frank, C. W. *Electronic Transitions and the High Pressure Chemistry and Physics of Solids*; John Wiley & Sons, New York, 1973.

(4) (a) Adams, D. M.; Long, G. J.; Williams, A. D. *Inorg. Chem.* **1982**, *21*, 1049. (b) Meissner, E.; Köppen, H.; Spiering, H.; Gütlich, P. *Chem. Phys. Lett.* **1983**, *95*, 163. (c) Pebler, J. *Inorg. Chem.* **1983**, *22*, 4125. (d) König, E.; Ritter, G.; Kulshreshtha, S. K.; Waigel, J.; Goodwin, H. A. *Inorg. Chem.* **1984**, *23*, 1896. (e) König, E.; Ritter, G.; Waigel, J.; Goodwin, H. A. *J. Chem. Phys.* **1985**, *83*, 3055. (f) Usha, S.; Srinivasan, R.; Rao, C. N. *Chem. Phys.* **1985**, *100*, 447. (g) Long, G. J.; Hutchinson, B. B. *Inorg. Chem.* **1987**, *26*, 608. (h) McCusker, J. K.; Zvagulis, M.; Drickamer, H. G.; Hendrickson, D. N. *Inorg. Chem.* **1989**, *28*, 1380. (i) Granier, T.; Gallois, B.; Gauthier, J.; Real, J.-A.; Zarembowitch, J. *Inorg. Chem.* **1993**, *32*, 5305. (j) König, E.; Ritter, G.; Grünstreudel, H.; Dengler, J.; Nelson, J. *Inorg. Chem.* **1994**, *33*, 837. (k) Roux, C.; Zarembowitch, J.; Itie, J.-P.; Polian, A.; Verdaguer, M. *Inorg. Chem.* **1996**, *35*, 574.

(5) (a) Hoselton, M. A.; Wilson, L. J.; Drago, R. S. *J. Am. Chem. Soc.* **1975**, *97*, 1722. (b) Katz, B. A.; Strouse, C. E. *J. Am. Chem. Soc.* **1979**, *101*, 6214. (c) Mikami-Kido, M.; Saito, Y. *Acta Crystallogr.* **1982**, *B38*, 452. (d) Binstead, R. A.; Beattie, J. K. *Inorg. Chem.* **1986**, *25*, 1481. (e) Konno, M.; Mikami-Kido, M. *Bull. Chem. Soc. Jpn.* **1991**, *64*, 339, 22. (f) Wiehl, L.; Kiel, G.; Köhler, C. P.; Spiering, H.; Gütlich, P. *Inorg. Chem.* **1986**, *25*, 1565.

(6) (a) Meissner, E.; Köppen, H.; Köhler, C. P.; Spiering, H.; Gütlich P. *Hyperfine Interact.* **1986**, *28*, 799. (b) Meissner, E.; Köppen, H.; Köhler, C. P.; Spiering, H.; Gütlich, P. *Hyperfine Interact.* **1987**, *36*, 1. (c) Köppen, H.; Meissner, E.; Wiehl, L.; Spiering, H.; Gütlich, P. *Hyperfine Interact.* **1989**, *52*, 29.

(7) Jeftić, J.; Romstedt, H.; Hauser, A. *J. Phys. Chem. Solids* **1996**, *57*, 1743.

(8) Jeftić, J.; Hinek R.; Capelli S. C.; Hauser, A. *Inorg. Chem.* **1997**, *36*, 3080.

(9) (a) König, E *Structure and Bonding* **1991**, *76*, 51. (b) Beattie, J. K. *Adv. Inorg. Chem.* **1988**, *32*, 1.

(10) (a) DiBenedetto, J.; Arkle, V.; Goodwin, H. A.; Ford, P. C. *Inorg. Chem.* **1985**, *24*, 456. (b) Adler, P.; Hauser, A.; Vef, A.; Spiering, H.; Gütlich, P. *Hyperfine Interact.* **1989**, *47*, 343. (c) Adler, P.; Spiering, H.; Gütlich, P. *J. Phys. Chem. Solids* **1989**, *50*, 587. (d) McGarvey, J. J.; Lawthers I.; Heremans K.; Toftlund, H. *Inorg. Chem.* **1990**, *29*, 252. (e) Wang, W.; Chan, I. Y.; Schenker, S.; Hauser, A. *J. Chem. Phys.* **1997**, *106*, 3817.

(11) Jeftić, J.; Hauser, A. *Chem. Phys. Lett.* **1996**, *248*, 458.

(12) Franke, P. L.; Haasnot, J. G.; Zuur, A. P. *Inorg. Chim. Acta* **1982**, *59*, 5.

(13) Wiehl, L. *Acta Crystallogr.* **1993**, *B49*, 289.

(14) Ozarowsky, A.; McGarwey, B. R. *Inorg. Chem.* **1989**, *28*, 2262.

(15) (a) Jung, J.; Bruchhäuser, F.; Feile, R.; Spiering, H.; Gütlich, P. *Z. Phys. B* **1996**, *100*, 517. (b) Jung, J.; Schmitt, G.; Wiehl, L.; Hauser, A.; Knorr, K.; Spiering, H.; Gütlich, P. *Z. Phys. B* **1996**, *100*, 523.

(16) Hauser, A. *Comments Inorg. Chem.* **1995**, *17*, 17.

(17) Hauser, A. *Chem. Phys. Lett.* **1992**, *192*, 65.

(18) Jeftić, J.; Kindler, U.; Spiering, H.; Hauser, A. *Meas. Sci. Technol.* **1997**, *8*, 479.
(19) Wiehl, L.; Spiering, H.; Gütlich, P.; Knorr, K. *J. Appl. Cryst.* **1990**, *23*, 151.
(20) (a) Willenbacher, N.; Spiering, H. *J. Phys. C: Solid State Phys.* **1988**, *21*, 1423. (b) Spiering, H.; Willenbacher, N. *J. Phys. Condens. Matter* **1989**, *1*, 10089.
(21) Spiering, H.; Meissner, E.; Köppen, H.; Müller, E. W.; Gütlich P. *Chem. Phys.* **1982**, *68*, 65.
(22) Adler, P.; Wiehl, L.; Meissner, E.; Köhler, C. P.; Spiering, H.; Gütlich, P. *J. Phys. Chem. Solids* **1987**, *48*, 517.
(23) Buhks, E.; Navon, G.; Bixon, M.; Jortner, J. *J. Am. Chem. Soc.* **1980**, *102*, 2918.
(24) Heller, E.; Ahsbahs, H.; Dehnicke, G.; Dehnicke, K. *Naturwissensch.* **1974**, *61*, 502.
(25) Donnelly, C. J.; Imbush, G. F. *NATO ASI Series B249* (DiBartolo, B., Ed.), Plenum Press: New York, 1991, p 175−195.
(26) Hauser, A.; Vef, A.; Adler, P. *J. Chem. Phys.* **1991**, *95*, 8710.
(27) Schläfer, H. L.; Gliemann, G. *Einführung in die Ligandenfeldtheorie*; Akad. Verlagsgesellschaft: Wiesbaden, 1980; p 462.
(28) Sugano, S; Tanabe, Y.; Kamimura, H. *Multiplets of Transition Metal Ions*, *Pure and Applied Physics 33*; Acad. Press: New York, 1970.
(29) Clack, D. W.; Smith, W. E. *J. Chem. Soc., Dalton Trans.* **1974**, 2015.
(30) Köhler, C. P.; Jakobi, R.; Meissner, E.; Wiehl, L.; Spiering, H.; Gütlich, P. *J. Phys. Chem. Solids* **1990**, *51*, 239.